

BIDIRECTIONAL INCHWORM MOTORS AND TWO-DOF ROBOT LEG OPERATION

Seth Hollar, Sarah Bergbreiter and K.S.J. Pister

Berkeley Sensor and Actuator Center, University of California, Berkeley 94720

ABSTRACT

We have demonstrated a bidirectional inchworm motor that produces equivalent forces in both directions. This motor uses an additional set of gap-closing-actuator arrays to pre-bias the drive frame. To obtain the highest force densities possible, the motors are designed close to the limiting resolution of the process. We describe the inequalities relating the lateral etch depth to the actuator gap spacing and tooth width of the inchworm motors.

In addition, we have demonstrated a two degree-of-freedom (DOF) robot leg operated with an external controller. The leg, 1 mm in length, was fabricated in a planarized SOI/2-poly process and was operated by two electrostatic inchworm motors. Each joint of the leg has demonstrated at least 90° of static angular deflection, and each inchworm motor has demonstrated a shuttle displacement of $400\ \mu\text{m}$ with speeds up to $6.8\ \text{mm/s}$. This corresponds to a robot foot speed of over $0.75\ \text{m/s}$ and over 4 full steps per second. Endurance tests have shown that the shuttle and leg are visually undamaged after 60,000 full leg sweeps for 16.5 hours of operation (~ 10 million inchworm cycles).

INTRODUCTION

In the past, researchers have demonstrated robot limb motion using either electrothermal or electrostatic actuation [1, 2, 3]. High power requirements prevent thermal actuators from being implemented on autonomous microrobots. Displacements from electrostatic actuation are generally limited by the gap spacing in the actuator. To overcome this limitation, Yeh demonstrated inchworm motors that convert the small displacements of gap closing actuator (GCA) arrays to large translations [4]. Using these inchworm motors, we previously reported a solar-powered 10 milligram robot [5]. The one-DOF legs and inchworm motors used in that robot were fabricated in a planarized SOI, two polysilicon layer process (SOI/2-poly process) [6]. This process allowed us to fabricate high force inchworm motors using the SOI device layer combined with polysilicon pin hinges for out-of-plane actuation.

This paper describes analysis methods and new microrobot components amenable to the SOI/2-poly process. To improve the force density of the actuators on our robot, we present an analysis of designing motors at the limits of the SOI/2-poly process. In addition, we demonstrate bidirectional inchworm motors to provide greater control over leg motion. Lastly, a new two-DOF robot leg has been designed and tested (Figure 1).

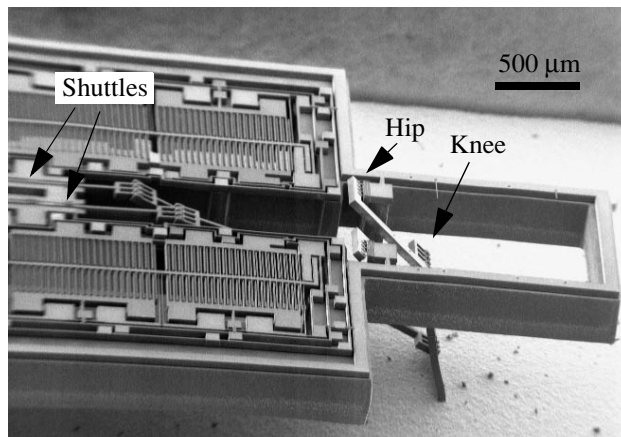


Figure 1. SEM of two-DOF leg. Leg is folded down and touching the bottom of the die package.

IMPROVING FORCE DENSITY

Process Considerations. In the SOI/2-poly process, a high-aspect-ratio advanced silicon etch (ASE) defines the inchworm motors in the SOI device layer. For high force density electrostatic actuators, it is desirable to have the smallest gap and thickest device layer possible. The thickness of the SOI device layer can be optimized based on the minimum resolution of the lithography and the aspect ratio of the ASE etch. Our lithography allows us to conveniently draw $2\ \mu\text{m}$ lines, and the ASE etch gives us an aspect ratio of 25:1. For device layers that are too thick, the aspect ratio during the ASE etch will widen the gap resulting in a loss of force density. For device layers that are too thin, the gap will not widen as much, but the force is lower due to the reduced actuation area from the thinner device layer. The best result is when the aspect ratio creates gaps on the order of the minimum resolution. In our case, we used SOI wafers with a $45\ \mu\text{m}$ thick device layer.

The ASE vertical etch in the device layer yields a small but non-zero lateral etch which is on the order of the minimum resolution of the lithography. The lateral etch affects backstop spacings, electrostatic gaps, and tooth widths in the inchworm motors. If the lateral etch can be predicted a priori, the design of the inchworm can be modified to account for this irregularity. In the next section, we discuss the effect lateral etching has on the inchworm motors.

Gap Spacing. Inchworm motors consist of two clutch/drive actuator pairs. Working in tandem, they translate the small displacements of the GCA arrays to large displacements of the shuttle. Figure 2 shows the Cadence layout of the clutch, shuttle, and backstop of an inchworm motor. Two clutch fin-

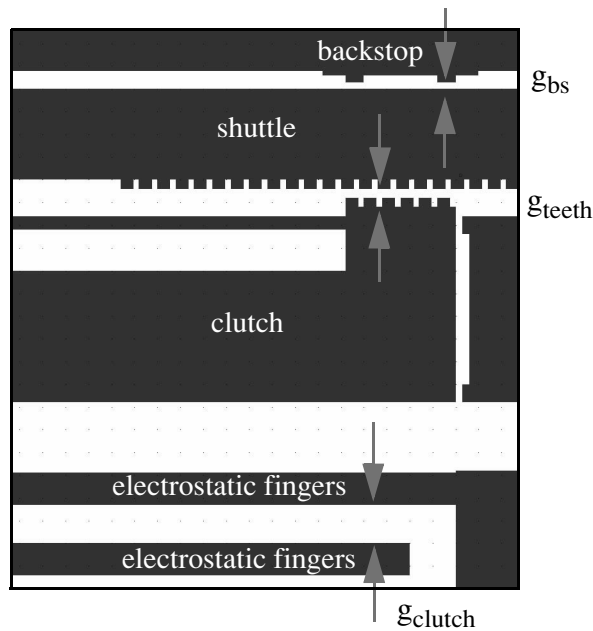


Figure 2. Layout of the backstop, shuttle, and clutch of an inchworm motor. Gap spacing between the shuttle and backstop (g_{bs}) and between the clutch and shuttle (g_{teeth}) dictate the minimum spacing between the GCA fingers (g_{clutch}).

gers are shown towards the bottom of the figure. The drawn gaps of the backstop, teeth, and clutch are g_{bs} , g_{teeth} , and g_{clutch} , respectively. It is important to remember that if a lateral etch uniformly etches the perimeter of the structures with a width of δ , the final gap spacing is an additional 2δ on top of the originally drawn gap width. To prevent shorting of the electrostatic fingers, the gap between the clutch GCA fingers must be larger with a sufficient margin than the sum total of the backstop gap and teeth gap.

This requirement is expressed by the inequality below:

$$(2\delta + g_{bs}) + (2\delta + g_{teeth}) < 2\delta + g_{clutch} \quad (1)$$

after simplification the inequality yields:

$$2\delta + g_{bs} + g_{teeth} < g_{clutch} \quad (2)$$

Here, we see that as the lateral etch increases, g_{clutch} must also increase to prevent finger shorting. In the SOI/2-poly process, we tailored the undercut so that $\delta = 0.5 \mu\text{m}$. With $g_{bs} = 1.5 \mu\text{m}$, and $g_{teeth} = 4 \mu\text{m}$, g_{clutch} must be greater than $6.5 \mu\text{m}$. In this case we made g_{clutch} $8.5 \mu\text{m}$ giving us a tolerance of $2 \mu\text{m}$.

Similar arguments follow for the drive actuator. In this case, there are only two gaps of interest. As Figure 3 shows, the final drive gap must be greater than the final backstop gap. Again with a lateral overetch of δ , we extract the following inequality:

$$2\delta + g_{bs} < 2\delta + g_{drive} \quad (3)$$

and simplifying we have:

$$g_{bs} < g_{drive} \quad (4)$$

The lateral etch on both gaps cancels out the effect. For our motors, $g_{bs} = 2.0 \mu\text{m}$ for the drive backstop and $g_{drive} = 4 \mu\text{m}$. Again, this gives a tolerance of $2 \mu\text{m}$.

For both the clutch and drive actuators, the effect of lateral etch also reduces the initial force the GCAs can produce. The inchworm's initial force comes from the drive actuators in their "normally open" position, the point where the gap distance is largest. This is determined by:

$$g_f = 2\delta + g_{drive} \quad (5)$$

Based on equation (5), the actual gap width, g_f , is $5 \mu\text{m}$ instead of the drawn gap of $4 \mu\text{m}$. This represents a 36% difference between the calculated force based on the drawn gap and the actual gap.

The force applied on the shuttle by the clutch is determined by the gap spacing of the clutch GCA array after the clutch has engaged. With a sufficient clutch force, the clutch will have pushed the shuttle fully against the backstops. In this case, the final electrostatic gap spacing is $2 \mu\text{m}$ which produces a force on the shuttle approximately 20x larger than the clutch's normally open position. With such a large increase in engagement force, the clutch GCAs can be designed to be substantially smaller than the drive GCAs of the inchworm actuators.

Gear Teeth. Furthermore, to ensure that force from the drive actuators is transmitted efficiently to the motor shuttle, we introduced gear teeth on the inchworm clutch and shuttle. If the gaps of the electrostatic actuators are fabricated at the minimum size, the pitch of the teeth is also limited to that distance. In this case, lateral etching plays a significant role in the teeth engagement between the clutch and shuttle.

To understand this mathematically, consider Figures 4a-c. The pictures give a close-up view of a clutch engaging the shuttle. In Figure 4a, the lateral etch of the device is assumed to be uniform around the perimeters of the structure defined with a lateral etch rate of δ . The drawn tooth width is α while the pitch of the teeth is Ω . To go through an entire inchworm cycle, each drive actuator needs to pull the shuttle half of a tooth pitch, $\Omega/2$. The actual toothwidth, T_w , is the drawn tooth width minus the lateral etch:

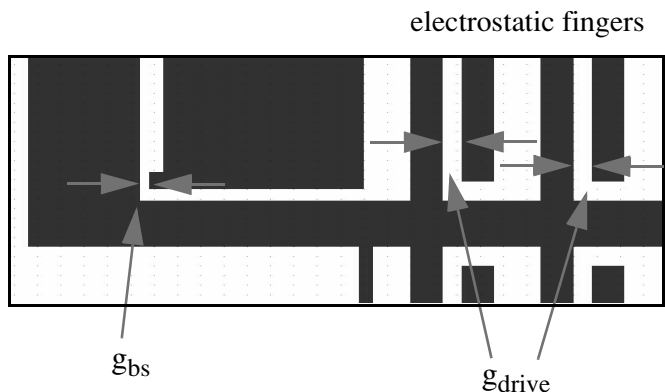


Figure 3. Layout of drive and drive backstop. Spacing of the gap between the backstop and drive frame dictates the minimum spacing between the GCA drive fingers.

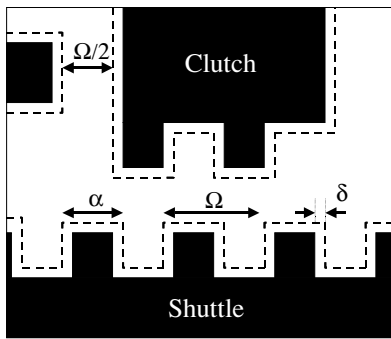


Figure 4. a) The drawn toothwidth is α , defined by the dotted outline. Due to a lateral etch of δ , the final toothwidth, T_w is $T_w = \alpha - 2\delta$ and the final gapstop spacing is $g_{\text{gapstop}} = \Omega/2 + 2\delta$.

$$T_w = \alpha - 2\delta \quad (6)$$

And the actual gapstop spacing is:

$$g_{\text{gapstop}} = \frac{\Omega}{2} + 2\delta \quad (7)$$

Figure 4b is a drawing of the clutch engaging the shuttle. While the inchworm motor operates, it goes through repeated cycles to accumulate large displacements on the shuttle. The clutch should engage the shuttle with a consistent forward spacing between the clutch and the shuttle teeth during each cycle. In Figure 4b, this spacing is denoted as γ .

In Figure 4c, the drive actuates, and the clutch moves forward against the gap stop. The clutch travels the width of the gap defined by the backstop, g_{gapstop} . The shuttle, however, does not move until the teeth make contact. The clutch first travels a distance, γ , before the shuttle is pulled forward. For periodic sequencing of the inchworm, the shuttle must travel exactly $\Omega/2$ in order for the next tooth engagement to also have a spacing of γ . Therefore we can setup the following equation:

$$g_{\text{gapstop}} - \gamma = \frac{\Omega}{2} + 2\delta - \gamma = \frac{\Omega}{2} \quad (8)$$

and simplifying:

$$\gamma = 2\delta \quad (9)$$

The forward spacing during engagement is twice the lateral etch of the device.

For the clutch to engage the shuttle, the actual width of the tooth plus the forward spacing, γ , must be less than the spacing between teeth. If not, the clutch teeth will not fit into the shuttle. We can setup the following inequality:

$$T_w + \gamma < \Omega - T_w \quad (10)$$

This simplifies with the help of equation (6) to:

$$\alpha < \frac{\Omega}{2} + \delta \quad (11)$$

Inequality (11) states that the drawn toothwidth must be less than half the period plus the lateral overetch. An additional restriction on the drawn toothwidth requires that the

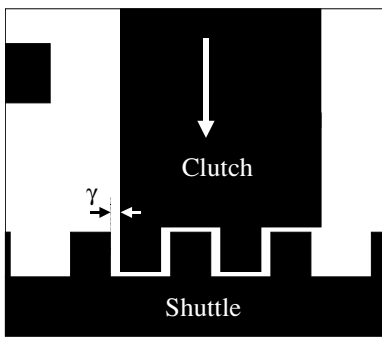


Figure 4. b) The clutch engages the shuttle. For periodic sequencing, the forward spacing between the clutch and the shuttle teeth should be consistent. This spacing is defined as γ .

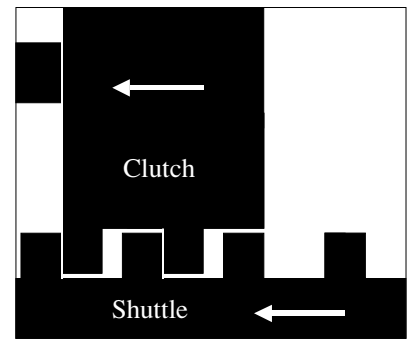


Figure 4. c) The drive finally moves the pawl forward against the gap stop. The pawl travels a g_{gapstop} distance while the shuttle travels $g_{\text{gapstop}} - \gamma$.

tooth is not completely etched away. This is represented simply enough by:

$$2\delta < \alpha \quad (12)$$

Combining the two inequalities yields boundary constraints on α :

$$2\delta < \alpha < \frac{\Omega}{2} + \delta \quad (13)$$

Assuming that a uniform lateral undercut is a reasonable first order estimate, we used (13) as a rule of thumb in designing tooth widths and pitches.

Rounding and lithography resolution can also affect the final shape and size of the gear teeth. Figure 5 shows a close-up SEM of the clutch and shuttle gear teeth. The gear teeth were drawn as rectangles but because their feature size was on the order of the minimum feature size of the process, the fabricated teeth were rounded. The rounded teeth can reduce the amount of “pulling” force the clutch can transfer to the shuttle. In our motors, the predominant failure was slipping between the clutch and shuttle teeth.

In our designs, we used a drawn tooth width of $2.8 \mu\text{m}$ and a $4 \mu\text{m}$ pitch. Although this violates the design conditions set forth in (13), the excessive rounding of the teeth still allowed the clutch and shuttle to engage reliably.

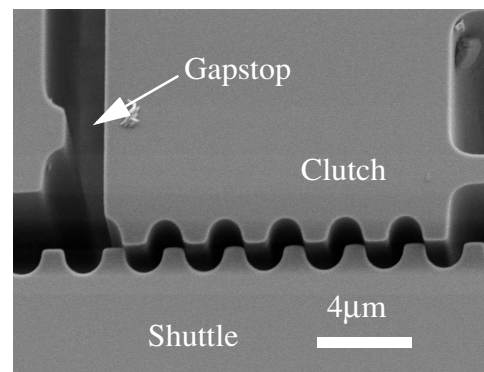


Figure 5. SEM of gear teeth. With this close-up shot of the gear teeth, one can notice that the teeth are no longer rectangular as they were drawn.

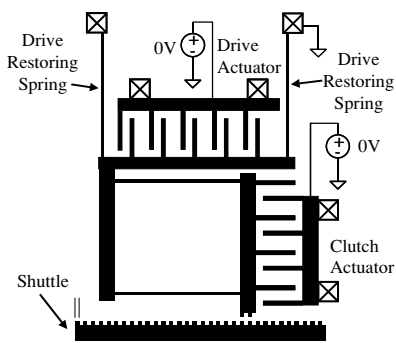


Figure 6. a) In the initial position both the clutch and drive actuators are at rest.

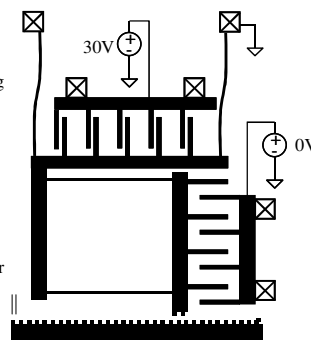


Figure 6. b) The drive actuator is preset before the clutch engages.

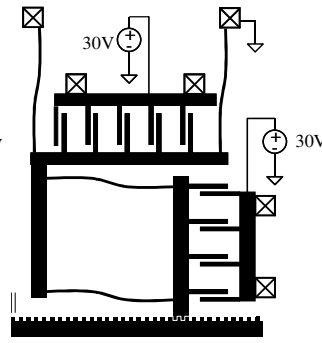


Figure 6. c) Clutch engages while drive is preset.

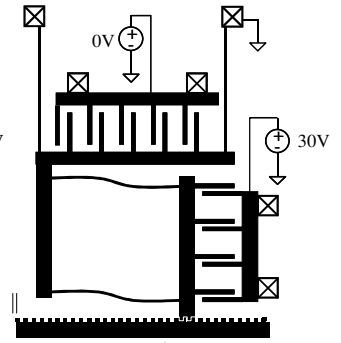


Figure 6. d) Turning off the drive actuator allows the drive restoring spring to pull the shuttle backwards.

In the next sections, we move away from the details of motor optimization to system level designs. In particular, we discuss two methods for reversing shuttle operation in an inchworm motor.

BIDIRECTIONAL INCHWORM ACTUATION

Method 1. One method to reverse the motion of the shuttle is to reverse the control sequence of the inchworm motor. Figure 6 shows just a single clutch/drive actuator pair, but this is sufficient to demonstrate the reversal mechanism. In the initial position, both the clutch and drive actuators are at rest (Figure 6a). The drive actuator is initially preset before the clutch engages (Figure 6b). Once the clutch engages, the drive is already preset so that the clutch engages the shuttle one half-pitch in the reverse direction (Figure 6c). Lastly, the electrostatic drive force is turned off allowing the restoring spring to force the shuttle in the reverse direction (Figure 6d).

The restoring force depends on the drive restoring spring (see Figure 6a). In the static view, the force of the spring should be greater than the load through at least half the period of motion, which is half the tooth pitch. As seen earlier, total displacement during actuation is larger than half a period of motion due to the etch in the lateral direction. As

previously defined, γ represents the forward spacing between teeth of the clutch and the shuttle. In a similar vein for reversing the motor, the same γ can be related to the maximum force the drive restoring springs can exert on the shuttle. In Figure 6b, the springs are preset a distance of:

$$g_{gapstop} = \frac{\Omega}{2} + 2\delta \quad (14)$$

If the drive restoring springs must pull the shuttle half the pitch, $\Omega/2$, then at the end of the restoring action in Figure 6d, the spring will be stretched $2\delta = \gamma$ at maximum. Therefore, the load must satisfy the following inequality for the inchworm to operate in the negative direction:

$$\gamma k_{spring} < F_{load} \quad (15)$$

where

k_{spring} is the spring constant of the drive restoring springs

F_{load} is the load on the shuttle

The two-DOF leg presented later is driven using this reversible mechanism. The drive restoring spring constant is $18 \mu\text{N}/\mu\text{m}$, and the lateral etch is $\delta = 0.5 \mu\text{m}$. According to (15), the shuttle load in the reverse direction is limited to $18 \mu\text{N}$.

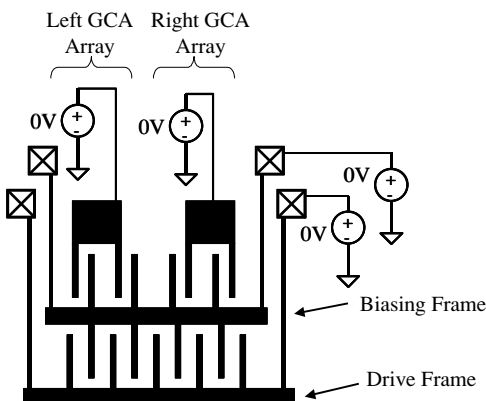


Figure 7. a) The diagram shows the right/left GCA arrays, the biasing frame, and the drive GCA array. Clutch GCA array not shown.

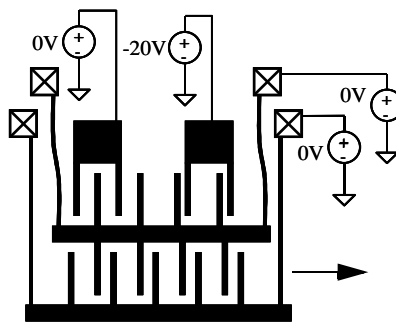


Figure 7. b) To move to the left, the biasing frame is first actuated to the right by applying a -20 V signal to the right GCA array. Gap stops not shown.

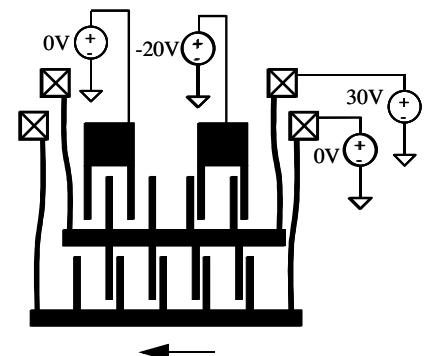


Figure 7. c) To move the drive frame to the left, a 30 V signal is then applied to the biasing frame.

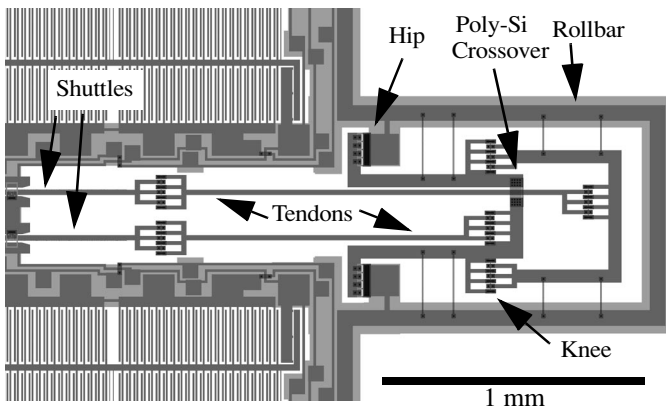


Figure 8. CAD drawing of two-DOF leg. Shuttles attach to the upper and lower legs through tendons. Hip and knee joints allow the leg to flex out of the plane

Method 2. A different inchworm design that has a minor effect on force density yet offers equivalent output force in both directions is shown below in Figure 7. The addition of two small sets of GCA arrays (left and right) enables one to bias the drive array for forward or reverse actuation. Figure 7a shows a cut out section of the motor that contains the drive array and biasing array. The clutch mechanics are identical to the original motor and therefore are not included in this figure.

In Figure 7b, the right GCA array is charged to -20 V, causing the biasing frame to actuate to the right. This places the drive electrodes closer to one set of the electrostatic fingers than the other. Gap stops (not shown) prevent the left/right GCA arrays from shorting. In Figure 7c, the drive frame is actuated forward by applying 30 V onto the biasing frame. The biasing GCA arrays are force decoupled from the engagement of the shuttle, so in the practical limit, they can be designed arbitrarily small. Therefore, the biasing GCA array need not have a large force, just enough force initially to move the biasing frame. Consequently, the biasing GCA array need only be a fraction the size of the drive GCA array, and therefore the force density of the actuator is not significantly degraded.

This motor design is complicated by the addition of two more signals and thus requires a more complex signal stream to drive the motors. If negative voltages are available, the biasing electrodes can be simply biased before a right or left motion commences. Then, the signal streams for the drive and clutch actuators can remain the same. If negative voltages are not available, the motors must be driven by switching all six signals during the inchworm cycle. For a unidirectional inchworm motor, only 4 steps are needed in a single cycle, but for the bidirectional motor, we used 8 steps for a single cycle.

TWO-DOF ROBOT LEG

While two one-DOF legs were used in the solar-powered robot [5], one can easily imagine designing more complex linkages through the SOI/2-poly process for future

robot designs. To this end, we have designed an inchworm actuated two-DOF leg. The leg uses two inchworm motors to drive two shuttles. Each shuttle is attached to a tendon which in turn moves an upper or lower leg linkage. The upper leg assembly is a slider-crank mechanical construct, and its orientation depends only on one of the shuttles. The lower leg is part of a 5-bar crank-slider construct, and its orientation depends on the positions of both shuttles.

The leg is realized in the CAD design shown in Figure 8. Polysilicon flaps constrain the motion of the shuttle to remain in the motor's plane. A rollbar designed in the SOI substrate is used to tether the legs in place and protect the legs during release and assembly. For future designs, as more degrees of freedom are implemented, crossover beams will be needed to bridge overlapping mechanical structures. In this case, only one polysilicon cross-over beam is used. The polysilicon cross-over beam (see Figure 8) bridges the lower leg structure overtop one of the tendons.

One way we simplified the mechanical design of the two-DOF leg over the one-DOF leg is the removal of the recoil spring which was required to re-initialize the motor shuttle. In this case, the shuttle is suspended only by the polysilicon flaps. Lifting the leg requires only enough force to overcome the friction of the flaps and hinges. This frictional force should be small compared to lifting a robot's weight. Since we require large forces in one direction and small forces in the other, we can simply reverse the driving sequence of the inchworm motors to lift the leg (bidirectional motor method 1). This is a good example of how we can reduce the complexity of the mechanical design by marginally increasing the complexity of the sequencing.

RESULTS

We have designed and tested a bidirectional inchworm motor (see Figure 9). Because this design was a test structure, the shuttle was suspended by a set of parallel flexures rather than driving a leg. The active area of the motor was fabricated in $1 \times 1.7 \text{ mm}^2$ and demonstrated both right and left motions at speeds up to 5.5 mm/s with a total travel of up to 224 μm in each direction. The motor was controlled by an external custom-made controller with positive voltages and 8 steps per cycle. The inchworm motor was driven with 40 V

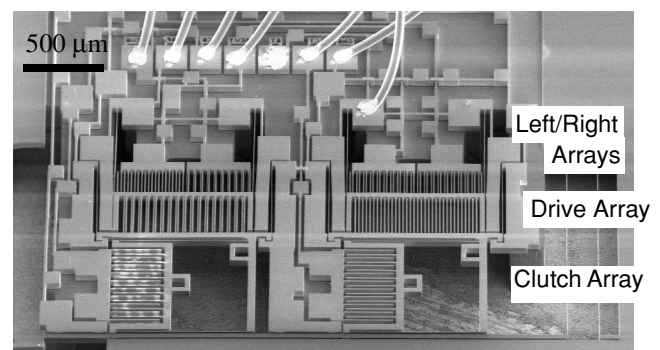


Figure 9. Bidirectional motor. The left/right GCA arrays bias the drive frame one way or the other to allow forward or reverse drive actuation.

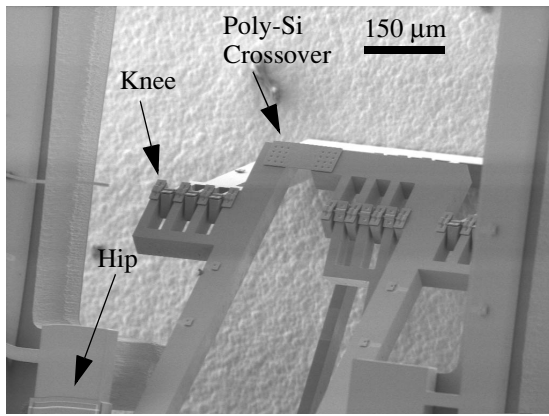


Figure 10. SEM close-up of the knee joint. Hinges comprise the joint connecting the legs and tendons together. Polysilicon cross-overs are used to bridge mechanical components.

for drive and clutch actuation, and 20 V for right/left GCA array actuation. With a spring constant of $0.08 \mu\text{N}/\mu\text{m}$, the maximum load on the motor was not more than $17.7 \mu\text{N}$.

We also fabricated a two-DOF leg operated with the same external controller (Figures 1 and 10). The segmented leg is 1 mm in total length and driven by two electrostatic inchworm motors. The entire device measures $6.1 \times 2.6 \text{ mm}^2$. The leg is composed of a “hip” joint and “knee” joint (Figure 10). Each joint was exercised with at least 90° of static angular deflection. The area swept out by the foot of the leg is more than 0.1 mm^2 (see Figure 11). Each inchworm motor was designed for and has demonstrated a shuttle displacement of $400 \mu\text{m}$ with speeds up to 6.8 mm/s ; a 70% improvement over previously reported results [4]. At this shuttle speed, the leg experiences an angular velocity of $1530^\circ/\text{s}$. These numbers correspond to a robot foot speed of over 0.75 m/s and a step rate of over 4 steps/s . The inchworm motor was driven using a 40 V drive and 50 V clutch actuation voltage. Reversing the leg motion was accomplished using the scheme outlined as Method 1. Reverse operation tests yielded nearly identical speeds to forward operation. In forward operation, the foot of the leg has exerted from $6 \mu\text{N}$ to $33 \mu\text{N}$ of vertical force, depending on

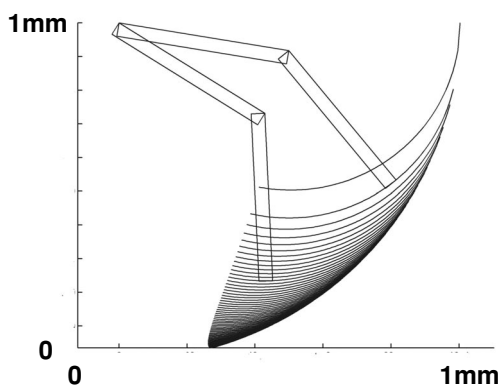


Figure 11. Area swept out by two-DOF leg. Lines represent sweeps of lower leg at a fixed upper leg angle. Tendons connect the moving shuttle to the upper and lower leg linkages.

the angle of the joints. The leg exerted larger forces the more it was deflected out of the plane. Shallower leg angles saw correspondingly lower forces. Endurance tests have shown that the leg and shuttle are visually undamaged after 60,000 full leg sweeps for 16.5 hours of operation (~ 10 million inchworm cycles).

CONCLUSIONS

We have 1) related performance of inchworm motors to the lateral etch in the SOI/2-poly process, 2) demonstrated reverse operation of inchworm motors with two different methods, and lastly 3) fabricated an inchworm actuated two-DOF leg. The motors of the leg are designed to output forces over $400 \mu\text{N}$, but clutch-shuttle slipping limits the leg force to $30 \mu\text{N}$. With improved gear tooth designs, however, the full force potential of the leg can be realized. While this paper focused on one type of leg, the SOI/2-poly process can easily realize a plethora of alternative multi-DOF leg designs. Combining the bidirectional motors mentioned here with these leg designs, we are moving closer to achieving the ultimate goal of multi-DOF, multi-legged microrobots.

ACKNOWLEDGEMENTS

We would like to thank Anita Flynn from MicroPropulsion Corp., Chris Keller from MEMS Precision Instruments, the Berkeley Microfabrication Facility and staff. This research is funded in part by DARPA/IPTO.

REFERENCES

- [1] P.E. Kladitis, V.M. Bright, “Prototype microrobots for micro-positioning and micro-unmanned vehicles”, *Sensors and Actuators A: Physical*, 80 (2000), pp.132-7.
- [2] T. Ebefors, J. Mattsson, E. Kalvesten and G. Stemme, “A micromotion system based on polyimide joint actuators,” *Euroensors XII*, 1998, pp. 391-4.
- [3] K. Suzuki, I. Shimoyama, H. Miura, and Y. Ezura, “Creation of an insect-based microrobot with an external skeleton and elastic joints,” in Proc. IEEE Workshop on Micro Electro Mechanical Systems (MEMS '92), Travemunde, Germany, Feb. 4-7, 1992, pp. 190-195.
- [4] R. Yeh, S. Hollar and K.S.J. Pister, “A single mask, large force and large displacement electrostatic inchworm motor,” *JMEMS*, vol. 11, no. 4 (August 2002), pp. 330-6.
- [5] S. Hollar, A. Flynn, C. Bellew and K.S.J. Pister, “Solar Powered 10 mg Silicon Robot,” *Digest of MEMS 2003*, Kyoto, Japan, 2003, pp. 706-11.
- [6] S. Hollar, A. Flynn, S. Bergbreiter and K.S.J. Pister, “Robot leg motion in a planarized SOI/2-poly process,” *Proceedings of the Solid-State Sensor, Actuator and Microsystems Workshop*, Hilton Head, SC, June 2002, pp. 54-8.